

Vibrational Assignments of *trans*-*N*-Methylacetamide and Some of Its Deuterated Isotopomers from Band Decomposition of IR, Visible, and Resonance Raman Spectra

X. G. Chen,[†] Reinhard Schweitzer-Stenner,^{‡,§} Sanford A. Asher,[†] Noemi G. Mirkin,[‡] and Samuel Krimm^{*,‡}

Department of Chemistry, University of Pittsburgh, Pittsburgh, Pennsylvania 15260, and Biophysics Research Division, University of Michigan, Ann Arbor, Michigan 48109

Received: October 31, 1994; In Final Form: November 28, 1994[⊗]

We have measured the IR absorption, Raman, and resonance Raman spectra of aqueous and neat *N*-methylacetamide (NMA) and its ND and CCD₃ isotopic derivatives and subjected them to a detailed line shape analysis. The amide I and II bands of NMA in H₂O are composed of at least two broad bands with different intensities and depolarization ratios. The two subbands of amide I are interpreted as arising from a vibrational mixing between the amide I vibration and the bending motion of water molecules hydrogen bonded to the peptide group. The amide II subbands most likely arise from two, nearly isoenergetic, NMA conformers, which differ in the orientation of the *N*-methyl hydrogens. In neat NMA conformational heterogeneity and a noncoincidence between the isotropic and anisotropic parts of the Raman tensor cause an even more complex structure of amide I. The amide III mode, even at visible excitation, and the band arising from the C–methyl symmetric bending motion exhibit depolarization ratios close to 0.33, which indicates that their intensities are entirely determined by the 190 nm $\pi \rightarrow \pi^*$ transition. The C-methyl symmetric bend is enhanced mainly by a CC stretch contribution. In contrast amide I and II show a dispersion of their depolarization ratios owing to additional contributions to their off-resonance spectra from electronic transitions at shorter wavelengths. The spectrum of the ND isotopic derivative exhibits an amide II' doublet at 1500 cm⁻¹, which results from a Fermi resonance interaction between the amide II' mode and a combination of amide IV' (632 cm⁻¹) and a skeletal deformation mode (873 cm⁻¹).

Introduction

N-Methylacetamide (CH₃CONHCH₃, NMA) is the simplest model system for investigating the structural and physical properties of the peptide group. Despite numerous studies,^{1–9} however, a detailed understanding of this simple molecule is only now emerging. Early X-ray diffraction data suggested that NMA is in the *trans* structure in the crystalline phase where its five heavy atoms are coplanar (*trans*- and *cis*-NMA refer to the orientation of CO and NH with respect to the CN bond).¹ NMR data,² UV resonance Raman experiments,^{3,4} and ab initio calculations⁵ indicate that NMA in aqueous solution is mainly *trans* but is in a thermodynamic equilibrium with the *cis* conformation, which is ca. 10 kJ/mol higher in free energy. Moreover, ab initio calculations on isolated NMA suggest that the *trans* conformer exists in four, nearly isoenergetic (i.e., $\Delta E < kT \approx 2$ kJ/mol) subconformations that differ in their methyl rotations with respect to the peptide group.⁶

Numerous spectroscopic studies have examined the vibrational dynamics of NMA. The classic infrared study by Miyazawa et al.⁷ provided a first understanding of the normal modes of NMA and other monosubstituted amides. The IR and Raman spectra are dominated by three bands in the mid-frequency range designated as amide I, II, and III that involve CO stretching, CN stretching, and NH in-plane bending motions. UV resonance Raman studies show that the amide II and III bands^{3,4,8,9} and also the amide I band^{10,11} are resonance enhanced by the amide $\pi \rightarrow \pi^*$ transition, which gives rise to a strong absorption band at 190 nm.

Recent work from our laboratories¹¹ has provided evidence through spectral decomposition that the amide I band of NMA in aqueous solution is composed of two broad subbands, at 1626 (I₁) and 1646 (I₂) cm⁻¹, which show different depolarization ratios. This pair of subbands can be rationalized in terms of mixing between the internal coordinates of NMA and the bending motion of water molecules hydrogen bonded to the peptide group.¹¹ In this study we extend this type of investigation to the entire high frequency region between 1200 and 1700 cm⁻¹ of NMA in H₂O, NMA in D₂O (NMAD), and neat NMA to elucidate the nature of the bands observed therein. In addition, IR and UV Raman spectra of the isotopic derivatives CD₃CONHCH₃ (CD₃-NMA) and the corresponding CD₃-NMAD were used to aid in the assignments. We used depolarization ratio measurements to infer the mechanism of resonance enhancement of the vibrational modes of NMA and NMAD. A consistent spectral analysis aids in identifying and assigning new features in the Raman spectra of these compounds. In particular, we find that the amide II band of aqueous NMA can be resolved into two subbands that result from different NMA conformers. This observation is in line with the interpretation⁶ of the earlier observed IR spectra of NMA in an Ar matrix taken at cryogenic temperature, which showed significant splitting of the major amide bands into up to four components.¹²

Materials and Methods

Materials. NMA was purchased from Sigma Chemical Co. and distilled before use. *N*-Methylacetyl-*d*₃-amide (CD₃-NMA) was synthesized by adding acetyl-*d*₃ chloride (Aldrich Chemical Co., 99% isotopic purity) to an excess of methylamine (Aldrich Chemical Co.) that was trapped at dry ice temperature. The purities of the final products were confirmed by proton NMR

[†] University of Pittsburgh.

[‡] University of Michigan.

[§] Permanent address: FB1–Institute of Experimental Physics, University of Bremen, 28359 Bremen, Germany.

* To whom correspondence should be addressed.

[⊗] Abstract published in *Advance ACS Abstracts*, February 1, 1995.

and mass spectra. D₂O (99.8%) was obtained from Cambridge Isotope Laboratories. NMA and CD₃-NMA were deuterated to form NMAD and CD₃-NMAD by dissolution in D₂O. The concentration of the analyte ranged between 2 and 3 M for IR and visible Raman measurements but was 0.5 M for the 238 nm UV Raman spectra.

Instrumental Methods. The 1064 nm excited IR Raman spectra and the IR absorption spectra were obtained by using a Nicolet 800 FT-IR spectrometer connected to a IR Raman accessory. The samples for IR Raman measurements were contained in quartz capillaries. The exciting laser beam was unpolarized. FT-IR spectra were measured using CaF₂ windows separated by a 15 μm Teflon spacer.

The Raman spectra were measured either at 90° or in a backscattering geometry. Excitations at 514, 457, and 363 nm were obtained from an argon ion laser. In all cases the incident laser beam was polarized perpendicular to the spectrometer optical axis. Measurements at 514 and 363 nm were carried out by focussing the incident laser beam by an *f* = 10 cm lens onto the sample. The scattered light was collimated and analyzed with a polarizer. A polarization scrambler was placed between the polarizer and the spectrometer's entrance slit. The scattered light was dispersed by a single SPEX 1701 0.75 m Czerny-Turner monochromator equipped with a 1200 grooves/mm grating. The 514 nm Rayleigh scattered light was rejected by using a holographic Raman notch filter manufactured by Kaiser Corp. The corresponding spectral resolution was 6 cm⁻¹ at 514 nm and 4 cm⁻¹ at 363 nm. The photons were detected by an intensified Reticon array. Measurements with 457 nm excitation used a 10 cm focal length lens to focus the laser beam on a quartz capillary, which was held at 30 °C. A lens with a 15° angular acceptance cone collected and focused the 90° scattered light on the entrance slit. A polarizer and polarization scrambler were used to examine the polarization. The scattered light was dispersed by a Spex Czerny-Turner double monochromator equipped with 2400 grooves/mm holographic gratings. The spectral resolution was 2 cm⁻¹.

UV excitations at 244 and 238 nm were obtained by intracavity frequency doubling of a CW argon laser.¹³ The UV light was focused onto the sample by a 10 cm focal length lens. The experiments were carried out in a backscattering geometry and by using a UV polarizer and a polarization scrambler. The details of the spectrometer are given elsewhere.¹⁰

All spectra were transferred to a personal computer and subjected to a line shape analysis by the program LabCalc (Galactic Instruments). The relative intensities of the Raman bands were derived from their areas. The depolarization ratio (*ρ*) was then calculated as:

$$\rho = I_{\perp}/I_{\parallel} \quad (1)$$

where *I*_⊥ and *I*_∥ denote the intensities measured with the polarizer oriented perpendicular and parallel to the incident polarization.

The accuracy of the depolarization measurements was checked by measuring the depolarization ratio of the totally polarized lines of CCL₄.¹⁴ The collection angle of the collimator is sufficiently small (15°) so that negligible errors occur in the determination of the depolarization ratios.¹⁵

Results and Discussion

The paper is organized as follows. Sections 1 and 2 describe the IR and UV resonance Raman spectra of NMA and some of its isotopic derivatives in terms of the normal modes of NMA-(H₂O)₂. Section 3 presents a spectral analysis of polarized and

depolarized Raman spectra of NMA, neat NMA, and NMAD. Section 4 discusses Raman enhancements from the π → π* transition and from electronic transitions at higher energies.

1. Normal Modes and IR Raman Spectra of NMA and Its Isotopic Derivatives. We have reexamined the vibrational spectra of NMA isotopomers in aqueous solution based on new normal mode calculations which utilize 4-31G* scaled ab initio force constants (Table 1). Normal modes were calculated for NMA-(H₂O)₂ complexes with one water molecule hydrogen bonded to the carbonyl oxygen and a second one to the amide hydrogen. In another calculation with the same basis set we examined the situation where a third water molecule was also hydrogen bonded to the carbonyl group.

Results from these ab initio calculations indicate that aqueous *trans*-NMA can exist in up to four conformations of planar symmetry, which differ in their *C*- and *N*-methyl orientations with respect to the CO and NH bonds. Similar results were obtained earlier for isolated⁶ and hydrogen-bonded^{5b} NMA. We designate these conformers as follows. NMA-N_cC_c means that the in-plane hydrogen of each methyl group is *cis* to the NH bond and the CO bond, respectively, while NMA-N_cC_t has the in-plane *N*-methyl hydrogen *cis* to NH and the in-plane *C*-methyl hydrogen *trans* to CO. Correspondingly, NMA-N_tC_t has hydrogens of both methyls *trans* to their reference bonds and NMA-N_tC_c has a *N*-methyl hydrogen in the *trans* and a *C*-methyl hydrogen in the *cis* configuration. The normal-mode compositions given in Table 1 have been calculated for the conformer N_cC_t, which is lowest in energy and therefore exhibits the largest occupation.

Figure 1 compares the 1064 nm excited IR Raman spectra of NMA and CD₃-NMA in H₂O, and NMAD and CD₃-NMAD in D₂O. The amide group gives rise to characteristic vibrations denoted amide I through VII; the *N*-deuterated derivatives have analogous vibrations which are designated with a prime (i.e., amide I' through VII'). Figure 1 shows that, in addition to the strong amide I, II, and III bands, aqueous NMA exhibits two other dominant lines at 632 (amide IV) and 883 cm⁻¹ which mainly involve skeletal deformation (skel d) resulting from a combination of NCH₃ r (r: rocking), CN s (s: stretching), CC s and CO ib (ib: in-plane bending) (Table 1). The weaker band at 448 cm⁻¹ is mainly CCN d with some contributions from CO ib and CCH₃ r. All these bands downshift upon deuteration of the *C*-methyl group (Figure 1b). *N*-deuteration causes a 10 cm⁻¹ downshift of the band at 882 cm⁻¹. The 1165 cm⁻¹ medium intensity band in the spectrum of NMA (Figure 1a) contains NCH₃ r and NC s. The overcrowded region between 1300 and 1700 cm⁻¹ in NMA shows the amide III band (1313 cm⁻¹, Figure 1a), the amide II band (at approximately 1580 cm⁻¹) and the amide I band (1626 cm⁻¹). Various methyl modes contribute to the unresolved features between 1400 and 1550 cm⁻¹. The spectroscopically isolated CCH₃ sb (sb: symmetric bending) band at 1377 cm⁻¹ (Figure 1a) arises mainly from symmetric CCH₃ sb, but the calculated potential energy distribution (PED)^{5,16} also shows some contributions from CCH₃ asymmetric bending (CCH₃ ab) and CC s (Table 1).¹⁷

N-deuteration drastically changes the spectrum (Figure 1c). Owing to the decoupling of NH ib and CN s, the amide III' band is found at 967 cm⁻¹. Amide I' appears nearly unchanged at 1626 cm⁻¹. The CCH₃ sb band is downshifted by approximately 6 cm⁻¹ to 1371 cm⁻¹ and its intensity is significantly reduced. Amide II' appears as a doublet at 1500 cm⁻¹ (Figure 2c), as reported earlier by Harada and Takeuchi.¹⁸ As shown in detail below, this doublet results from a Fermi resonance interaction between amide II' and the combination mode of amide IV' at 632 cm⁻¹ and the skel d mode at 873 cm⁻¹.

TABLE 1: Observed and Calculated Frequencies (in cm^{-1}) of Some Modes of Aqueous Hydrogen-Bonded NMA, $\text{CD}_3\text{-NMA}$, NMAD, and $\text{CD}_3\text{-NMAD}$

mode ^a	$\nu(\text{obs})$	$\nu(\text{calc})$	potential energy distribution ^b
NMA-(H ₂ O) ₂ ^c			
Am I ₂	1646	1632	CO s(39) (O)HOH b(35) (H)HOH b(11) CN s(10) CCN d(6)
		1631	(O)HOH b(54) CO s(19) (H)HOH b(16)
Am I ₁	1626	1628	(H)HOH b(86) CO s(17)
Am II	1580 ^d	1580	NH ib(45) CN s(41) CO ib(8) NC s(8) CC s(7)
NCH ₃ ab	1474	1469	NCH ₃ ab(83) NCH ₃ r(10) NCH ₃ sb(6)
NCH ₃ oab	1453	1443	NCH ₃ oab(94) NCH ₃ or(8)
CCH ₃ oab		1436	CCH ₃ oab(91) CCH ₃ or(8)
CCH ₃ ab	1434	1444	CCH ₃ ab(61) CCH ₃ sb(17) NH ib(7)
NCH ₃ sb	1416	1421	NCH ₃ sb(93) NC s(5)
CCH ₃ sb	1377	1381	CCH ₃ sb(66) CCH ₃ ab(24) CC s(8)
Am III	1313	1303	NH ib(30) CN s(18) CCH ₃ sb(17) CO ib(11) CC s(6) CO s(5) NH \cdots O ib(5)
	1165	1173	NCH ₃ r(50) NC s(13) CNC d(8) CO s(7) NCH ₃ ab(6)
	1105	1097	NC s(52) CCH ₃ r(12) CC s(9) NCH ₃ r(9) CO ib(5)
Skel d	883	880	NCH ₃ r(22) CN s(19) CC s(15) CNC d(9) CO ib(8) NC s(7) CCN d(6) CO s(6)
Am V		745	NH \cdots O ob(41) CN t(38) NH ob(22) H \cdots OH b(13) H \cdots OH b(13)
Am IV	632	637	CO ib(35) CC s(34) CNC d(7) NC s(5)
	447	443	CCN d(52) CO ib(30) CCH ₃ r(13) CNC d(8)
NMA-(H ₂ O) ₃			
Am I ₂	1646	1634	CO s(43) (O)HOH b(24) (H)HOH b(14) CN s(13) CCN d(7)
Am I ₁	1626	1628	(O)HOH b(34) CO s(31) (H)HOH b(18) CCN d(5)
$\text{CD}_3\text{-NMA-(H}_2\text{O)}_2$ ^c			
H ₂ O		1631	(O)HOH b(89)
H ₂ O		1629	(H)HOH b(103) CO s(6)
Am I	1619	1622	CO s(72) CCN d(11) CN s(10) (H)HOH b(9) NH ib(6)
Am II	1584 ^d	1579	CN s(45) NH ib(45) CO ib(8) NC s(8) CC s(5)
NCH ₃ ab	1472	1468	NCH ₃ ab(86) NCH ₃ r(9) NCH ₃ sb(6)
NCH ₃ oab	1453	1443	NCH ₃ oab(95) NCH ₃ or(8)
NCH ₃ sb	1416	1421	NCH ₃ sb(94) NCH ₃ ab(6) NC s(6) CO s(5)
Am III	1334	1328	NH ib(37) CN s(19) CC s(19) CO ib(12) NH \cdots O ib(6) NCH ₃ sb(5)
	1165	1172	NCH ₃ r(52) NC s(12) CNC d(9) CO s(6) NCH ₃ ab(6)
CCD ₃ sb	1117	1121	CCD ₃ sb(39) NC s(31) CC s(21)
CCD ₃ ab	1040	1042	CCD ₃ sb(32) NC s(30) CCD ₃ ab(21) NCH ₃ r(7) CO ib(6)
Skel d	872	868	NCH ₃ r(18) CC s(15) CO ib(12) CCD ₃ sb(10) CNC d(9) CCN d(9) CO s(8) CN s(7)
	802	803	CCD ₃ r(62) CN s(11) CO ib(7)
Am V		740	NH \cdots O ob(44) CN t(38) NH ob(26)
Am IV	594	591	CC s(35) CO ib(24) NC s(5) CCD ₃ r(5)
	409	408	CCN d(35) CO ib(29) CCD ₃ r(20) CNC d(14) CO \cdots H b(8)
NMAD-(D ₂ O) ₂ ^c			
Am I'	1626	1624	CO s(75) CN s(23) CCN d(10) CCH ₃ r(5)
Am II' ₂	1516 } 1493 }	1518 } 1504 }	CN s(41) CCs(19) CO ib(13) ND ib(12) NC s(9) CO s(7)
Am II' ₁			in Fermi resonance with 872 + 632
NCH ₃ ab	1476	1468	NCH ₃ ab(87) NCH ₃ r(10) NCH ₃ sb(5)
NCH ₃ oab	1451	1443	NCH ₃ oab(94) NCH ₃ or(8)
CCH ₃ oab		1436	CCH ₃ oab(91) CCH ₃ or(8)
CCH ₃ ab	1436	1430	CCH ₃ ab(70) NCH ₃ sb(14) CCH ₃ sb(6)
NCH ₃ sb	1412	1415	NCH ₃ sb(85) NC s(11) CCH ₃ ab(8) CN s(5) NCH ₃ ab(5)
CCH ₃ sb	1371	1374	CCH ₃ sb(88) CCH ₃ ab(10)
	1185	1180	NCH ₃ r(49) (O)DOD b(12) ND ib(6) CO ib(6) NCH ₃ ab(6) CNC d(6)
	1125	1137	NC s(43) CCH ₃ r(14) ND ib(11) CC s(9)
Am III'	967	950	ND ib(55) CCH ₃ r(18) CN s(10) ND \cdots O ib(9)
Skel d	873	868	NCH ₃ r(21) CN s(16) CC s(16) NC s(11) CNC d(8) CO ib(7) CCN d(6) ND ib(5)
Am IV'	632	634	CO ib(36) CC s(33) CNC d(7)
Am V'		529	ND \cdots O ob(44) ND ob(36) CN t(33) D \cdots OD b(13) D \cdots OD b(13) CO ob(6)
	448	439	CCN d(52) CO ib(30) CCH ₃ r(12) CNC d(9)
$\text{CD}_3\text{-NMAD-(D}_2\text{O)}_2$ ^c			
Am I'	1616	1616	COs (79) CN s(22) CCN d(11)
Am II'	1501	1510	CN s(48) CC s(17) CO ib(14) ND ib(14) NC s(10) CO s(6)
NCH ₃ ab	1469	1468	NCH ₃ ab(86) NCH ₃ r(9) NCH ₃ sb(6)
NCH ₃ oab		1443	NCH ₃ oab(95) NCH ₃ or(9)
NCH ₃ sb	1411	1416	NCH ₃ sb(98) NC s(9)
	1197	1193	(D)DOD b(43) NCH ₃ r(23) (O)DOD b(8) CC s(7) ND ib(6)
	1120	1146	NC s(37) CCD ₃ sb(18) NCH ₃ r(17) CC s(16) ND ib(5)
CCD ₃ sb	1050	1050	CCD ₃ sb(52) NC s(15) CCD ₃ ab(7) ND ib(7) CN s(6) CO ib(5)
CCD ₃ ab		1026	CCD ₃ ab(89) CCD ₃ sb(5)
Am III'	971	962	ND ib(47) NC s(22) ND \cdots O ib(8)
Skel d	860	855	NCH ₃ r(19) CC s(15) CO ib(11) ND ib(10) CCD ₃ sb(9) CNC d(8) CCN d(8) CO s(6) CN s(6)
	802	798	CCD ₃ r(61) CN s(12) CO ib(7)
Am IV'	594	588	CC s(34) CO ib(25) CNC d(5) CCD ₃ r(5)
Am V'		516	ND ob(33) ND \cdots O ob(31) CO ob(25) CCD ₃ or(23) CN t(16)
	409	403	CCN d(38) CO ib(32) CCD ₃ r(21) CNC d(15)

^a Am: amide; ab: in-plane antisymmetric bend; oab: out-of-plane antisymmetric bend; sb: symmetric bend; skel d: skeletal deformation. ^b s: stretch; b: bend; ib: in-plane bend; ob: out-of-plane bend; r: in-plane rock; or: out-of-plane rock; t: torsion. (O)HOH: water molecule hydrogen bonded to carbonyl oxygen; (H)HOH: water molecule hydrogen bonded to amide hydrogen. All contributions to the PED larger than 5 are listed. For definition of symmetry coordinates see ref 6. ^c The wavenumbers between 1200 and 1800 cm^{-1} were obtained from the decomposed spectra measured at 457 nm excitation. Wavenumbers between 400 and 1200 cm^{-1} were obtained by the spectral analysis of the IR Raman spectrum.^d The apparent frequency of amide II. The frequencies of the subbands are given in the text. ^e The wavenumbers were taken from the IR Raman spectrum.

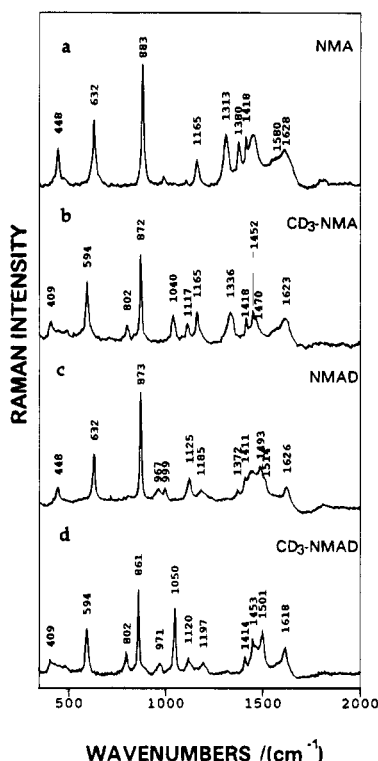


Figure 1. Aqueous IR Raman spectra of (a) NMA, (b) CD₃-NMA, (c) NMAD, and (d) CD₃-NMAD. The concentrations of the samples were 1.0 M. The frequency values label the observed peak positions of the Raman bands. Therefore they can be somewhat different from the values obtained from the spectral analysis.

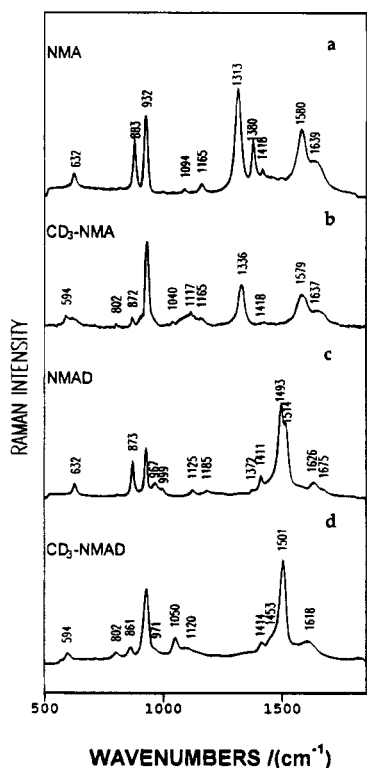


Figure 2. Aqueous UV resonance Raman spectra of (a) NMA, (b) CD₃-NMA, (c) NMAD, and (d) CD₃-NMAD measured at 238 nm excitation. The concentrations of the samples were 0.5 M. The frequency values label the observed peak positions of the Raman bands. Therefore they can be somewhat different from the values obtained from the spectral analysis.

Deuteration of the *C*-methyl group shifts its symmetric deformation mode to much lower frequencies (1117 cm⁻¹, Figure 1d). Amide III shifts up to 1335 cm⁻¹ because the CCH₃

sb contribution is eliminated. The alterations of the broad features between 1400 and 1500 cm⁻¹ are discussed in section 3.

2. UV Resonance Raman Spectra of NMA and Its Isotopic Derivatives. Figure 2 displays the preresonance UV Raman spectra of aqueous NMA, CD₃-NMA, NMAD, and CD₃-NMAD measured at 238 nm excitation. Only a few NMA bands show resonance enhancement by the ca. 190 nm $\pi \rightarrow \pi^*$ transition, namely skel d, amide III, CCH₃ sb, and the dominating amide II band, which is comparatively weak with near infrared excitation (Figure 1a). Amide I is enhanced and appears as a shoulder on amide II. Wang et al.^{9a} concluded from their resonance excitation profile (REP) of amide I that this band is not enhanced by the $\pi \rightarrow \pi^*$ transition. However, our recent measurements of the amide I REP¹⁰ and depolarization ratio¹¹ indicate strong $\pi \rightarrow \pi^*$ resonance enhancement. Similar to NMA, the amide I, II and III bands are resonance enhanced in CD₃-NMA, while the CD₃ sb band at 1117 cm⁻¹ (cf. Figure 1) is not resonance enhanced by the $\pi \rightarrow \pi^*$ transition (Figure 2).

The NMAD UV Raman spectrum (Figure 2) shows a dominant enhancement of the 1493 and 1516 cm⁻¹ amide II' doublet band. The 873 cm⁻¹ band, which is strong with IR Raman excitation, decreases its relative intensity at higher excitation energies in the UV.¹⁰ Amide I' and the methyl bands between 1500 and 1600 cm⁻¹ become comparatively weak. As we have shown earlier,¹⁰ some of these weak bands may get some part of their intensity from the $\pi \rightarrow \pi^*$ transition of NMA and NMAD.

3. Spectral Decomposition and Determination of Depolarization Ratios. We measured polarized and depolarized Raman spectra of aqueous NMA, neat NMA and NMAD with visible and UV excitation (Figures 3–5). Spectral decomposition was carried out after subtracting corresponding reference spectra of pure H₂O or D₂O. This eliminates the background and the H₂O Raman band at ca. 1640 cm⁻¹, which overlaps the amide I band. The neat NMA spectra were only slightly corrected by subtracting a linear background. All clearly resolved lines (e.g., amide III, II, I and CCH₃ sb) were best fit to a mixed Gaussian–Lorentzian band shape. Corresponding Raman bands in the spectra observed with different excitation wavelengths were consistently fit with identical band shapes and half-widths. Slight deviations in the band positions (± 3 cm⁻¹) were allowed to account for some uncertainties in the calibration of the spectra, but the same frequencies were used to fit corresponding bands in the polarized and depolarized spectra measured with the same excitation wavelength. Such spectral analysis reveals a rather complex structure of the spectra, which has not been previously recognized. The frequencies, half-widths, and depolarization ratios of all lines thus obtained are listed in Tables 2–4.

(a) *Amide I.* We demonstrated previously¹¹ that the amide I band of aqueous NMA is composed of two broad subbands at 1626 cm⁻¹ (I₁) and 1646 cm⁻¹ (I₂) with half-widths of 45 and 48 cm⁻¹, respectively. The Q values of these bands differ in the visible but approach 0.33 at 244 nm excitation. Their intensity ratio, $R(I) = I(I_2)/I(I_1)$, also depends strongly on the excitation wavelength. I₁ is more intense in IR absorption, IR and visible Raman spectra (Figures 6, 1, and 3, respectively), while I₂ dominates with UV excitation (cf. Figures 2 and 3). This observation rules out the possibility that these bands are due to conformational heterogeneity, because we find that corresponding normal modes of different NMA conformers have very similar eigenvectors.

Our normal-mode calculations on the NMA-(H₂O)₂ complex show that the amide I vibration is mixed with the HOH bending

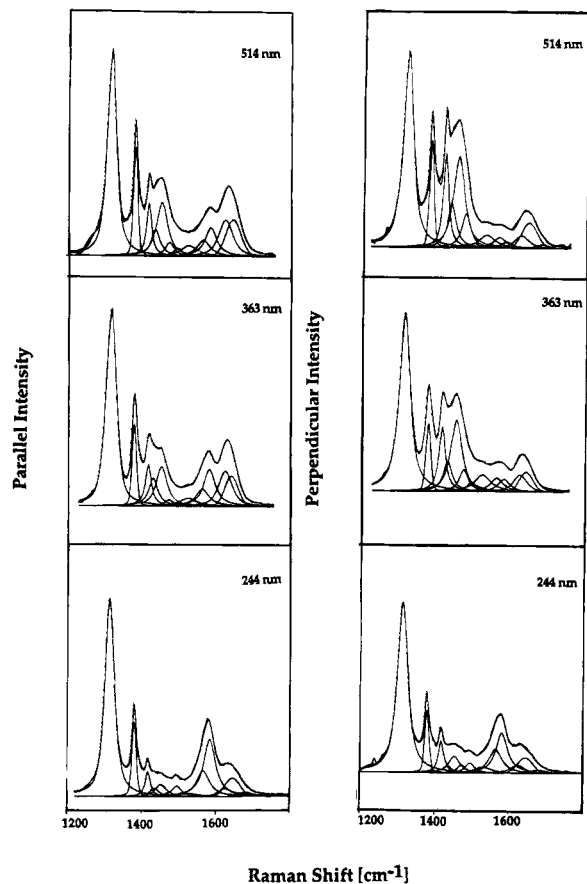


Figure 3. Polarized (left column) and depolarized (right column) Raman spectra of NMA in H₂O measured at 514, 363, and 244 nm excitation. The concentrations of the samples were 2 M. The depolarized spectra were scaled by 0.3 to permit comparison with the corresponding polarized spectra. The single bands displayed therein result from the line-shape analysis outlined in the text. The dotted points represent the experimentally observed spectra.

vibrations of the hydrogen-bonded water molecules. This interaction splits amide I into three modes, whose frequencies are calculated to be 1628, 1630, and 1632 cm⁻¹ for N_cC_t and 1628, 1631, and 1632 cm⁻¹ for N_cC_t, respectively. We also performed calculations on a NMA-(H₂O)₃ complex¹¹ with two water molecules hydrogen bonded to the CO group¹⁹ and obtained two amide I vibrations at 1628 and 1634 cm⁻¹ for the N_cC_t conformer.

While the predicted splitting is relatively insensitive to the NMA conformation, it is much smaller (4 cm⁻¹ for NMA-(H₂O)₂ and 6 cm⁻¹ for NMA-(H₂O)₃) than our observed difference between the amide I subbands (20 cm⁻¹). Two possible mechanisms may be responsible for this discrepancy. One reason for the underestimation of the splitting may stem from an incomplete modeling of the hydrogen-bonded H₂O molecules. The CO- and NH-bonded waters undoubtedly belong to clusters of H₂O molecules. Intermolecular coupling can be expected to mix the HOH bending vibrations of different water molecules in such a cluster, thus giving rise to a distribution of energy states. This idea is supported by the large half-width of the H₂O Raman band at 1640 cm⁻¹, viz., ≈110 cm⁻¹ (data not shown). The amide I mode will interact with a range of HOH bending modes of such clusters, which could result in larger splittings than those predicted by our three-water calculations. In other words, a NMA-H₂O cluster system must be regarded as the dynamic entity.

Another possible explanation for the large splitting may be a higher order resonance interaction between such coupled amide I-H₂O modes, which can be described by quartic terms in the

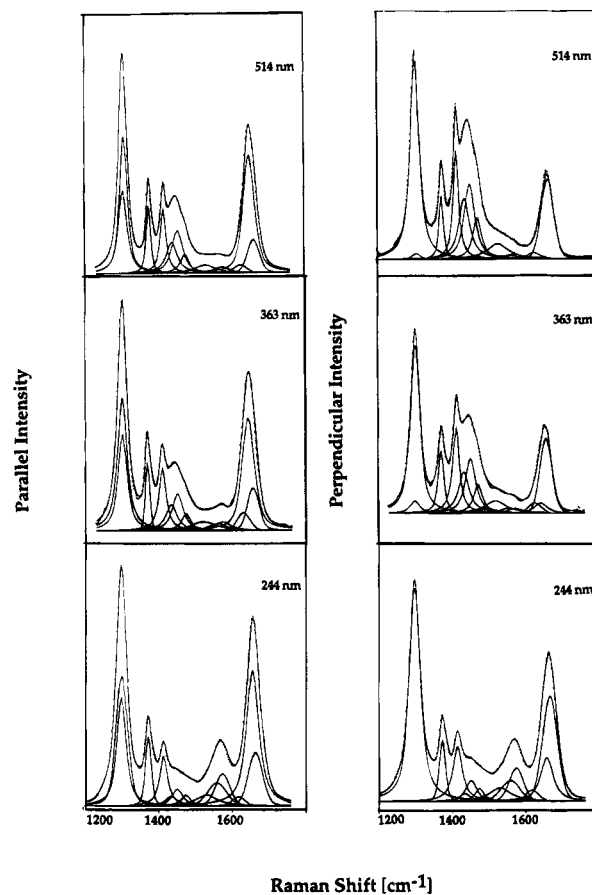


Figure 4. Polarized (left column) and depolarized (right column) Raman spectra of neat NMA measured at 514, 363, and 244 nm excitation. The depolarized spectra were scaled by 0.33 (514 nm), 0.4 (363 nm), and 0.37 (244 nm) to permit comparison with the corresponding polarized spectra. The single bands displayed therein result from the line-shape analysis outlined in the text. The dotted points represent the experimentally observed spectra.

expansion of the potential energy.²⁰ Such a coupling is likely because these modes have several internal coordinates in common, which allows anharmonic coupling between them to occur. To check whether this idea would be consistent with our experimental data, we utilized the results of the normal coordinate analysis of the NMA-(H₂O)₂ system in the following way. This calculation yields three amide bands at 1626, 1631, and 1632 cm⁻¹. The eigenvectors of their normal modes can be used to estimate that part of their relative intensity which results from the π → π* transition by employing the method described in our earlier work¹⁰ (a brief description is given in section 4). This yields relative intensities of 1:10:3 for the 1626, 1631, and 1632 cm⁻¹ bands, respectively. The last two bands are nearly identical in frequency, so that we can represent them by a single band (I₂) which is 13-fold more intense than the 1626 cm⁻¹ band (I₁).

This ratio is significantly larger than the corresponding measured intensity ratio of 2.2 obtained from the 244 nm excited spectrum. It should be noted that at this wavelength the intensities of both amide I bands are dominated by the π → π* transition. We now invoke the above higher order resonance interaction and assume that the unperturbed intensity ratio $R_0 = I_0(I_2)/I_0(I_1)$ of the two amide I subbands is indeed 13. The interaction changes this intensity ratio to a value R , which can be calculated from²¹

$$R(I) = \frac{I(I_2)}{I(I_1)} = \frac{(\sqrt{R_0} \cos \alpha + \sin \alpha)^2}{(\cos \alpha - \sqrt{R_0} \sin \alpha)^2} \quad (2)$$

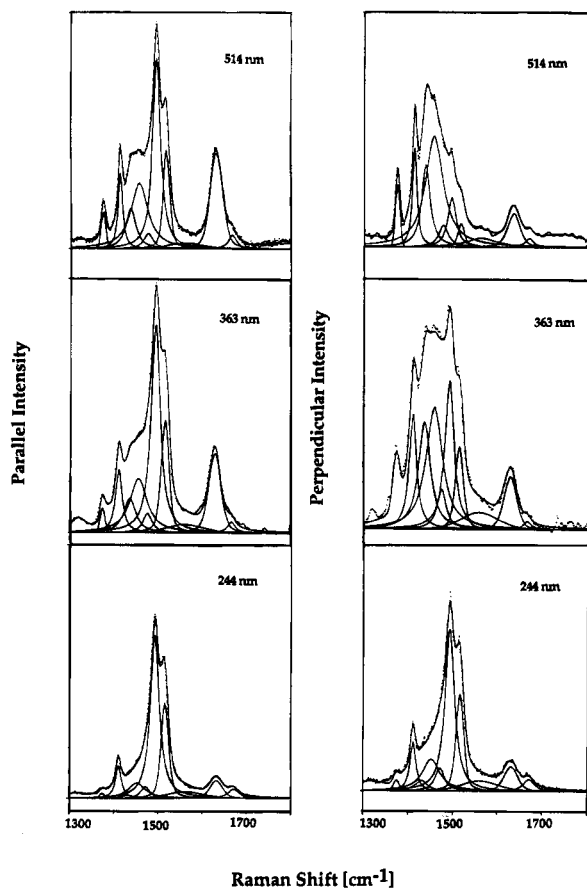


Figure 5. Polarized (left column) and depolarized (right column) Raman spectra of aqueous NMAD measured at 514, 363, and 244 nm excitation. The concentrations of the samples were 2 M. The depolarized spectra were scaled by 0.4 (514 nm), 0.3 (363 nm), and 0.375 (244 nm) to permit comparison with the corresponding polarized spectra. The single bands displayed therein result from the line-shape analysis outlined in the text. The dotted points represent the experimentally observed spectra.

TABLE 2: Frequencies (ν), Half-Widths (Γ), and Depolarization Ratios (ρ)^a of Raman Bands in the Spectra of NMA in H₂O

mode	ν [cm ⁻¹]	Γ [cm ⁻¹]	ρ_{514}^b	ρ_{457}^b	ρ_{363}^b	ρ_{244}^b
Am III	1313	28	0.36	0.30	0.36	0.35
CCH ₃ sb	1377	14	0.35	0.32	0.32	0.31
NCH ₃ sb	1416	20	0.63	0.62	0.6	0.5
CCH ₃ ab	1434	33	0.5	0.7	0.4	0.3
NCH ₃ oab	1453	35	0.58	0.56	0.6	0.5
NCH ₃ ab	1474	28	0.8	0.7	0.7	0.7
Am II (cis)	1496	29	0.2	0.3	0.3	0.3
	1526	53	0.4	0.5	0.7	0.7
Am II ₁	1566	42	0.2	0.2	0.3	0.34
Am II ₂	1584	37	0.1	0.1	0.1	0.26
Am I ₁	1626	45	0.12	0.14	0.17	0.36
Am I ₂	1646	48	0.24	0.22	0.23	0.32

^a Depolarization ratios with one significant figure are less certain due to the low intensities of the bands. ^b The subscript denotes the excitation wavelength.

where

$$\alpha = \frac{1}{2} \arctan(-2W/\delta\nu_0) \quad (3)$$

$$W = \frac{1}{2} \sqrt{(\delta\nu^2 - \delta\nu_0^2)} \quad (4)$$

$\delta\nu_0$ and $\delta\nu$ are the differences between the unperturbed and experimentally observed frequencies, respectively. W is the interaction energy and α reflects the degree to which the involved states are mixed. If one takes $\delta\nu_0 = 4 \text{ cm}^{-1}$ (as

TABLE 3: Frequencies (ν), Half-Widths (Γ), and Depolarization Ratios (ρ)^a of Raman Bands in the Spectra of Neat NMA

mode	ν [cm ⁻¹]	Γ [cm ⁻¹]	ρ_{514}^b	ρ_{457}^b	ρ_{363}^b	ρ_{244}^b
Am III aniso ^c	1302	29	0.32	0.34	0.33	0.35
Am III iso	1304	25				
CCH ₃ sb	1371	13	0.31	0.38	0.33	0.31
NCH ₃ sb	1413	19	0.52	0.55	0.53	0.44
CCH ₃ ab	1438	34	0.64	0.56	0.75	0.3
NCH ₃ oab	1452	34	0.61	0.73	0.61	0.42
NCH ₃ ab	1473	29	0.7	0.7	0.7	0.4
Am II (cis)	1493	30	0.4	0.6	0.5	0.4
	1529	68	0.5	0.7	0.6	0.4
Am II ₁	1566	47	0.4	0.3	0.3	0.3
Am II ₂	1579	47	0.3	0.3	0.2	0.3
Am I ₁	1630	42	0.24	0.34	0.26	0.33
Am I ₂ iso ^c	1646	37	0.15	0.18	0.21	0.26
Am I ₂ aniso	1658	36				

^a Depolarization ratios with one significant figure are less certain due to the low intensities of the bands. ^b The subscript denotes the excitation wavelength. ^c We calculated the apparent depolarization ratio by dividing the total intensity measured perpendicular and parallel to the incident polarization.

TABLE 4: Frequencies (ν), Half-Widths (Γ), and Depolarization Ratios (ρ)^a of Raman Bands in the Spectra of NMAD

mode	ν [cm ⁻¹]	Γ [cm ⁻¹]	ρ_{514}^b	ρ_{363}^b	ρ_{244}^b
CCH ₃ sb	1371	13	0.61	0.73	0.66
NCH ₃ sb	1412	13	0.49	0.49	0.39
CCH ₃ ab	1436	27	0.6	0.8	0.8
NCH ₃ oab	1451	47	0.6	0.5	0.5
NCH ₃ ab	1476	25	0.5	0.5	0.3
Am II' ₁ ^c	1493	21	0.10	0.18	0.26
Am II' ₂ ^c	1516	18	0.10	0.18	0.26
	1570	100	0.59	0.50	0.42
Am I'	1626	22	0.13	0.16	0.32

^a Depolarization ratios with one significant figure are less certain due to the low intensities of the bands. ^b The subscript denotes the excitation wavelength. ^c Am II'₁ and Am II'₂ are two lines of a Fermi resonance doublet.

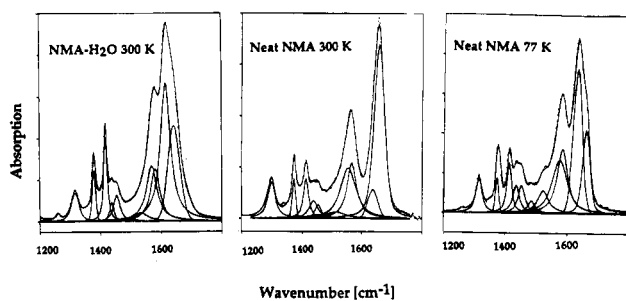


Figure 6. IR spectra of aqueous NMA (left column), neat NMA at 300 K (middle column), and neat NMA at 77 K (right column). The concentrations of the samples were 2 M. The single bands displayed therein result from the line-shape analysis outlined in the text. The dotted points represent the experimentally observed spectra.

predicted by the normal coordinate analysis of the NMA-(H₂O)₂ complex) and a positive sign for the interaction energy one obtains $R = 0.5$. A larger initial splitting of 10.0 cm^{-1} yields $R = 1$. If one also allows a somewhat smaller observed splitting of $\delta\nu = 16 \text{ cm}^{-1}$, which would still be within the limits of experimental accuracy, one obtains $R = 1.3$. Even though these calculated ratios are smaller than the experimentally determined value of 2.2, this rather crude estimation shows that such resonance interaction could at least be partially responsible for the large amide I splitting and also for the large relative intensity of the I₁ subband.

In NMAD the DOD bending modes are at much lower frequencies than the corresponding H₂O vibrations and coupling

with amide I' cannot occur. As expected, the NMAD spectrum shows only one comparatively narrow amide I' band at 1626 cm^{-1} with a half-width of 33 cm^{-1} (Figure 5). This finding also agrees nicely with results from the ab initio calculations, which yield frequency values of 1626 cm^{-1} for the N_2C_1 and 1625 cm^{-1} for the N_1C_1 conformer of NMAD, thus predicting a splitting of only 1 cm^{-1} .

The amide I mode of neat NMA is upshifted and more intense than that of NMA in H_2O . The spectrum of neat NMA is similar to that of NMA in non-hydrogen-bonding solvents in that amide I is upshifted in frequency and has a much greater intensity.⁹ We observe that the polarized and depolarized components of amide I have significantly different frequencies viz., 1646 and 1658 cm^{-1} , respectively (cf. Figure 4). A self-consistent fit to both components requires bands which we designate as $I_2(n)$ (1646 cm^{-1}) and $I_3(n)$ (1658 cm^{-1}). While $I_2(n)$ is nearly totally polarized ($\rho < 0.03$), $I_3(n)$ is depolarized with $\rho = 0.75$. Only $I_3(n)$ appears in the IR spectrum of neat NMA.

The totally different polarization properties of $I_2(n)$ and $I_3(n)$ provide considerable evidence that the amide I mode has different frequencies for the isotropic and anisotropic parts of its Raman tensor. This phenomenon is generally termed a noncoincidence effect (NCE). It is well known in the physics of pure liquids and binary mixtures and has been observed for many diatomic molecules,²² compounds with a carbonyl group,²³ dimethyl sulfoxide,²⁴ 1,2,5-thiadiazole,²⁵ chloroform,²⁶ and monoamides such as formamide²⁷ and *N,N*-dimethylacetamide.²⁸ Theoretical work has shown that the NCE is due to resonant transfer of vibrational energy between adjacent molecules. It arises from combined effects of anisotropic intermolecular interactions, which bring about an orientation dependent interaction potential,²⁹ and specific interactions between the identical vibrations of adjacent molecules through transition dipole coupling.^{29,30} Hence those modes with large transition dipole moments can be expected to show the largest NCE. Normally this interaction causes a red-shift, which is larger for the isotropic than for the anisotropic part of the Raman band, so that its polarized and depolarized components are no longer at the same frequency. This is what we observe for amide I in neat NMA.

The NCE can be described as a type of vibrational mixing of degenerate modes that causes a splitting into in-phase and out-of phase vibrations.³¹ Only the in-phase vibration is active in the isotropic Raman spectrum, while both components show up in the anisotropic Raman spectra.²⁹ A single IR band is predicted to occur close to the depolarized Raman band.^{29d,e} This exactly characterizes the amide I subbands $I_2(n)$ and $I_3(n)$ of neat NMA. The splitting observed for amide I of NMA in H_2O may also be understood as a special type of NCE. It differs from the interaction in neat NMA because the interacting modes (amide I and HOH bend) are not identical in terms of frequency, transition dipole strength, and symmetry. As a consequence, the splitting into in-phase and out-of phase components does not totally unmix the isotropic and anisotropic scattering and ρ is therefore less different than is found for amide I in neat NMA. Thus, we observe a collective delocalized amide I motion within neat NMA oligomers as well as for NMA-water clusters.

To obtain a perfect fit to the entire region between 1600 and 1640 cm^{-1} , we required an additional band at 1630 cm^{-1} , which is designated $I_1(n)$. This band is weak and polarized in the Raman spectrum and of intermediate intensity in the IR spectrum of neat NMA. It becomes very strong in IR spectra taken at cryogenic temperatures (Figure 6). At present we have no specific assignment for subband $I_1(n)$ in the spectrum of neat NMA; it is rather weak in the visible and UV Raman spectra and a little stronger in the corresponding IR absorption spectrum (Figure 6). Interestingly, it increases in intensity with decreasing

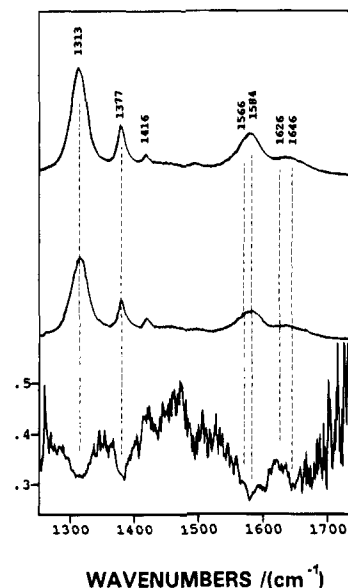


Figure 7. Intensity ratio I_{\perp}/I_{\parallel} of the aqueous NMA Raman spectra between 1300 and 1700 cm^{-1} measured with 244 nm excitation (lower curve). The corresponding polarized (upper curve) and depolarized spectra (middle curve) are shown for comparison and orientation.

temperature and becomes predominant at 77 K (Figure 6). It may reflect the presence of a different oligomeric form in the NMA network.

(b) *Amide II.* For aqueous NMA the amide II band is comparatively weak in Raman spectra excited in the visible or near IR, where it appears as a shoulder on amide I, but becomes intense at 244 nm (Figure 3). A consistent fit to the parallel and perpendicular polarized amide II bands requires a decomposition into two rather broad subbands, II_1 and II_2 centered at 1566 and 1584 cm^{-1} ($\pm 4\text{ cm}^{-1}$) with half-widths of 42 and 38 cm^{-1} , respectively. The corresponding intensity ratio $R(\text{II}) = I(\text{II}_2)/I(\text{II}_1)$ varies between 1.4 at 514 nm and 1.9 at 244 nm . Two such subbands also appear in the UV Raman spectra of $\text{CD}_3\text{-NMA}$ as judged by a line shape analysis of these data (not shown).

The amide II band in the IR absorption spectrum of aqueous NMA can also be well fitted by the above "two subband model" (Figure 6). The intensity ratio of 0.8 is somewhat different from that obtained for the corresponding subbands in the Raman spectra.

It is difficult to resolve two bands whose frequency difference is equal to or smaller than half their half-widths,³² but in our case the resolution is facilitated by the fact that both bands differ in their ρ values (Table 2), which vary with excitation wavelength. This is clear from Figure 7 which shows the ratio of the 244 nm depolarized to the polarized Raman spectra. The intensity ratio is close to 0.3 in the amide I region. It varies between 0.28 and 0.26 on the high-frequency side and at the maximum of the amide II band (1582 cm^{-1}), and increases toward 0.33 on the lower energy side of this Raman band, where there is a shoulder at 1558 cm^{-1} . This clearly suggests that amide II consists of more than one band, and a consistent fit to the polarized and depolarized spectra requires at least two subbands with different depolarization ratios.

Two explanations can be given for this amide II subband pair. First, one might try to assign it to a Fermi resonance interaction of amide II with a combination or overtone. A check of possible combinations reveals, however, that none matches the frequency region of amide II, so that one would be forced to invoke very large anharmonicities in order to justify this explanation. Therefore, we do not believe that Fermi resonance coupling provides a reasonable explanation of our data. Second, one

could assume that the amide II subbands result from different NMA conformations. In principle this possibility is supported by our present 4-31G* ab initio calculations on *trans*-NMA-(H₂O)₂ complexes. As mentioned earlier, these calculations provide evidence for the existence of NMA conformers that differ in terms of the orientation of their methyl hydrogens. We find for NMA-(H₂O)₂ that the energy levels of these conformers are arranged in the order N_cC_t < N_tC_t < N_cC_c < N_tC_c. However, the calculations show that only two of these conformers (i.e., N_cC_t and N_tC_t) represent true minima with respect to all the NMA coordinates. This is corroborated by calculations with a 6-31+G* basis set, which yield optimized structures with real frequencies only for these two conformers.¹⁶

The normal mode calculations for these two conformers yield amide II frequencies of 1580 cm⁻¹ for N_cC_t and 1593 cm⁻¹ for N_tC_t. These values are higher than the experimentally determined frequencies of the subbands, but the splitting of 13 cm⁻¹ accounts for 70% of the experimentally observed splitting of 18 cm⁻¹ for aqueous NMA. For aqueous CD₃-NMA the theoretical splitting is 14 cm⁻¹ while the experimental value is 20 cm⁻¹. Interestingly, the calculations predict a significantly smaller splitting for amide III (4 cm⁻¹), which would account for its smaller bandwidth.

The energy difference between the above two conformers is calculated to be 1.2 kJ/mol, which is significantly less than *kT* (2.4 kJ/mol) at room temperature. Thus one expects that the intensity ratio of the amide II subbands will depend only weakly on temperature. The temperature dependence of the relative intensity ratio is difficult to determine experimentally because alterations in temperature also affect the frequencies and half-widths of both the amide I and II subbands. An unambiguous assessment of all these changes will require the measurement of polarized and depolarized Raman spectra at different temperatures and excitation wavelengths.

In NMAD, amide II' appears as a doublet of relatively narrow component bands at 1493 and 1516 cm⁻¹, each of 24 cm⁻¹ half-width (Figure 5). In contrast to our assignment of amide II of NMA, we interpret this doublet as being caused by a Fermi resonance interaction between amide II' and the combination of the amide IV' and skel d modes. The IR Raman spectrum in Figure 1 shows that the combination of amide IV' and the strong 873 cm⁻¹ skel d band adds up to 1505 cm⁻¹, which is just in the center of the amide II' doublet. The intensity ratio of the two bands (i.e., $R(\text{II}') = I(\text{II}'_2)/I(\text{II}'_1) = 0.38$) is independent of the excitation wavelength (Figure 5). The ρ values of the bands are identical at all excitation wavelengths. The doublet is absent in the spectra of CD₃-NMAD (Figure 1) and NMAD with the *N*-methyl group deuterated.^{3d} The N_cC_t and N_tC_t conformers would not result in an amide II' doublet since our ab initio calculations predict an amide II frequency splitting of only 5 cm⁻¹, which would not be resolved.

The identical depolarization ratios further suggest that the unperturbed combination band itself has a negligibly small intensity. In this case the difference $\delta\nu_0$ between the unperturbed amide II' band and the combination band can be calculated by^{33a,b}

$$\delta\nu_0 = \frac{1 - R(\text{II}')}{1 + R(\text{II}')} \quad (5)$$

With the observed $\delta\nu = 23$ cm⁻¹ one obtains $\delta\nu_0 = 10.3$ cm⁻¹. Since the Fermi resonance frequency shift is equal in magnitude for each unperturbed band,²⁰ the unperturbed amide II' mode is predicted to be at 1510 cm⁻¹ and the unperturbed combination band of the skel d and amide VI modes would be at 1499 cm⁻¹, which is only 6 cm⁻¹ less than the sum of the frequencies inferred from the IR Raman spectrum shown in

Figure 1. This shows that the unperturbed combination band itself is not significantly anharmonic.

Inserting the above $\delta\nu_0$ and $\delta\nu$ values into eq 4, one obtains a Fermi resonance interaction energy *W* of 10.3 cm⁻¹, which is in the range of typical Fermi resonance coupling values.^{33b}

In the Raman spectrum of neat NMA with visible excitation amide II is unfortunately weak, so that its spectral decomposition is difficult. However, it is clearly detectable in the UV Raman (Figure 4) and the FT-IR absorption spectra (Figure 6). A consistent fit to all these data sets can again be made if one invokes two subbands, which are positioned at 1566 and 1579 cm⁻¹, but in contrast to the situation with aqueous NMA we feel that the present data do not allow us to suggest an unambiguous assignment, in particular because it is likely that both the NCE and structural heterogeneity affect the amide II band.

(c) *Amide III*. The aqueous NMA amide III band at 1313 cm⁻¹ is narrower than amide II and has a half-width of 30 cm⁻¹ (Figure 3). ρ is very close to 0.33 at all excitation wavelengths, which indicates that the $\pi \rightarrow \pi^*$ transition at 190 nm dominates the Raman scattering of this line even far from resonance (section 4). While this band dominates the visible Raman, and together with amide II also the UV Raman spectra, it is relatively less intense in the IR absorption spectrum (Figure 6a). In NMAD the amide III' band is at a much lower frequency and is significantly less intense.

In neat NMA the amide III band is slightly narrower (25 cm⁻¹) than in aqueous NMA and appears at 1303 cm⁻¹ (Figure 4). Such a frequency downshift is generally interpreted as indicative of weaker hydrogen bonding to the NH group. Interestingly, we found that the perpendicular component of amide III in neat NMA is slightly downshifted, by 2 cm⁻¹, with respect to the parallel polarized band. Both components differ in half-width, i.e., 29 cm⁻¹ for the perpendicular and 25 cm⁻¹ for the parallel polarized band. The IR spectrum displays a single band close to the position of the depolarized Raman band (i.e., 1300 cm⁻¹, Figure 6). This is again indicative of a NCE, but amide III shows a somewhat different behavior in that its NCE is smaller and has its anisotropic part at lower frequencies. Such a reversed NCE has already been observed for CO s of methanol by Torii and Tasumi³⁰ and has been rationalized in terms of transition dipole coupling between neighboring molecules whose relative position and orientation are determined by hydrogen bonding.

(d) *Spectral Region between 1370 and 1500 cm⁻¹*. The most intense bands in this region at 1377 and 1416 cm⁻¹ in aqueous and neat NMA (Figures 3 and 4) are assigned to the symmetric deformation vibrations of the CCH₃ (CCH₃ sb) and NCH₃ (NCH₃ sb) groups, respectively. Both bands downshift slightly in NMAD (Figure 5). For aqueous and neat NMA, ρ of CCH₃ sb is close to 0.33, while the band becomes more depolarized in NMAD and this $\rho > 0.6$ becomes independent of the excitation wavelength. The NCH₃ sb bands of NMA in water, neat NMA and NMAD show $\rho > 0.6$ in the visible, but ρ decreases with UV excitation (Table 2).

The region between 1420 and 1500 cm⁻¹ of aqueous NMA and neat NMA can be resolved into four bands at 1434, 1453, 1474, and 1496 cm⁻¹ (Figures 3 and 4), which based on the normal coordinate analysis^{5,16} (Table 1) and their depolarization ratios (Tables 2 and 3) can be assigned to in-plane asymmetric CCH₃ bending (CCH₃ ab, 1434 cm⁻¹), out-of-plane asymmetric NCH₃ bending (NCH₃ oab, 1453 cm⁻¹), in-plane asymmetric NCH₃ bending (NCH₃ ab, 1474 cm⁻¹) and the amide II mode of *cis*-NMA.^{3c,4} We would not exclude the possibility that since the out-of-plane CCH₃ asymmetric bending (CCH₃ oab) is very close in frequency, it may contribute to the 1434 cm⁻¹ band.

One may question the assignment of the band at 1453 cm^{-1} to NCH_3 oab in view of the fact that the remaining out-of-plane modes do not contribute to the visible and UV Raman spectra. However, other possible interpretations turn out to be much less convincing. First of all, its insensitivity to the isotopic substitutions utilized in this study suggests that it is governed by *N*-methyl vibrations. Hence one might suspect that this band results from the conformational heterogeneity discussed above. In that case one would expect that it arises from *N*-methyl ab modes of the N_cC_t conformer, which we indeed calculate to downshift by approximately 8 cm^{-1} with respect to the N_cC_t conformer (1469 cm^{-1}), to which we assign the band at 1474 cm^{-1} . However, to account for the intensity ratio of the bands at 1474 and 1453 cm^{-1} , and since the occupation of N_cC_t is a factor of 1.5 larger than that of N_tC_t , one has to assume that the intrinsic Raman cross section of the supposed NCH_3 ab band of N_tC_t is 10 times larger than that of N_cC_t . This is physically unreasonable since the eigenvectors are very similar. Moreover, the observed wavenumber difference (21 cm^{-1}) is 2.5-fold larger than the calculated splitting between the NCH_3 modes of the above conformers. Finally, the 1474 cm^{-1} band practically disappears in the IR spectra of aqueous and neat NMA, while the 1453 cm^{-1} band still prevails. Taken together, the above observations practically rule out the possibility that the 1453 cm^{-1} band stems from the N_cC_t conformer and we are left with its assignment to the NCH_3 oab vibration. The CCH_3 ab band of N_cC_t is expected to lie somewhere between the 1453 and 1474 cm^{-1} bands.

All the asymmetric methyl modes have large depolarization ratios ($\rho > 0.5$) with visible excitation. It should be noted that, for aqueous and neat NMA (Table 2), ρ of CCH_3 ab decreases significantly with UV excitation, whereas it stays depolarized in NMAD (Tables 3 and 4). Changes in ρ of the asymmetric *N*-methyl modes are within the limit of accuracy (Tables 2–4).

(e) *Assignment of Raman Band near 1530 cm^{-1} .* Decomposition of the spectra of aqueous and neat NMA between 1500 and 1600 cm^{-1} requires a broad ($60\text{--}80\text{ cm}^{-1}$) depolarized band centered at 1526 cm^{-1} . This band is most obvious in perpendicular polarized spectra of neat NMA, where it is comparatively strong (Figure 4).

At present we can only provide tentative assignments of this band. Its large half-width may indicate that it is composed of different subbands, which cannot be resolved from the present data. This band can be assigned to overtones and combinations. Possible candidates in aqueous and neat NMA are combinations of the Raman bands at 448 and 1097 cm^{-1} (1545 cm^{-1}) and 632 and 883 cm^{-1} (1515 cm^{-1}). For $\text{CD}_3\text{-NMA}$ a combination of the bands at 409 and 1115 cm^{-1} would provide a band at 1524 cm^{-1} . For NMAD, which shows this band at 1570 cm^{-1} , the combination could be 1125 and 448 cm^{-1} (1573 cm^{-1}).

4. Interpretation of Depolarization Ratios. If the Raman cross section is mainly determined by a single nondegenerate electronic transition, one component of the Raman tensor dominates and $\rho = 0.33$.³⁴ This is exactly what we observe for amide III and CCH_3 sb of aqueous and neat NMA at all excitation wavelengths. In agreement with our earlier conclusions from an analysis of UV resonance excitation profiles,¹⁰ this shows that these bands get their intensity exclusively from the $\pi \rightarrow \pi^*$ transition, even for excitation in the visible. In NMAD, however, the situation differs in that the CCH_3 sb band is now depolarized ($\rho \approx 0.75$) with visible and UV excitation. This shows that it is not enhanced by the $\pi \rightarrow \pi^*$ excitation, in agreement with our earlier conclusions.¹⁰

The ρ values of the amide I and II subbands are smaller than 0.33 in the visible but approach this value in the UV. This shows that for visible excitation the intensities of amide I and II are less dominated by the ca. 190 nm $\pi \rightarrow \pi^*$ transition, which dominates on approaching preresonance in the UV at 244 nm excitation. ρ values smaller than 0.33 indicate that the Raman tensor has at least two components of identical signs, which requires at least two electronic transitions with different directions of their transition dipole moments. In the case of amide I and II it is likely that this additional transition may be the one giving rise to the absorption band observed at 160 nm .^{3a}

Most of the methyl bands between 1400 and 1500 cm^{-1} have $\rho > 0.4$ at all excitation wavelengths. This indicates that their Raman tensor has at least two components with different signs.^{34a} In aqueous NMA the ρ values of NCH_3 sb at 1417 cm^{-1} and CCH_3 ab at 1434 cm^{-1} decrease with UV excitation. The latter approaches 0.33 in the preresonance UV region. This observation indicates that these modes are also getting some intensity from the $\pi \rightarrow \pi^*$ transition. While this effect is even stronger for NCH_3 ab of NMAD, it is totally absent for CCH_3 ab.

The different $\pi \rightarrow \pi^*$ resonance enhancements of the NMA and NMAD methyl modes can be understood if one considers the relative displacements Δ_i of the π^* state along their normal coordinates (Q_i). The Raman cross section is proportional to Δ_f^2 .³⁵ We have recently used the eigenvectors L_{ij} of the normal coordinates of aqueous NMA and NMAD,¹⁰ together with the resonance excitation profiles of some Raman bands, to determine the changes Δ_j in the corresponding *j*th internal coordinate. These were determined from the overall displacements $\Delta_i = \sum_j L_{ij}\Delta_j$ along Q_j in the $\pi \rightarrow \pi^*$ transition. The present depolarization ratio data are consistent in that they suggest that CCH_3 sb is enhanced by the $\pi \rightarrow \pi^*$ transition in aqueous NMA mainly because of a significant CC s contribution to its normal coordinate. The lack of resonance enhancement for CCH_3 sb in NMAD is caused by the reduction and the sign change of the CC s contribution, which is positive in NMA but negative in NMAD. This gives rise to a cancellation effect in NMAD, where the added contributions of CN s, CO s, and NC s are nearly compensated for by CC s. The NCH_3 sb mode behaves differently, in that it is more resonance enhanced in NMAD than in aqueous NMA. This occurs because CN s and NC s provide larger contributions to the NCH_3 sb mode of NMAD.

These findings contradict the earlier proposal by Spiro and co-workers,^{9a,36} who explained the resonance enhancement of CCH_3 sb of NMA (designated as amide S in their paper) by vibrational mixing with amide III. This explanation is inaccurate, because in the harmonic case normal modes of the same molecule do not mix with each other. What occurs instead is coupling between *local* coordinates, which mix and contribute to the PEDs and eigenvectors of different normal modes, though with different amplitudes and signs. Normal coordinate analysis gives specific contributions of these coordinates to amide I, II, III, CCH_3 sb, and NCH_3 sb. Such analysis indicates that these modes become resonance enhanced because they all have contributions from CN s, CO s, CC s, and NC s, which are involved in the geometry changes in the $\pi \rightarrow \pi^*$ transition.¹⁰

Altogether the above results demonstrate the validity of the displacement parameters derived in ref 10. They thus strongly corroborate the notion that although the π^* excited state geometry differs between hydrogen-bonded and non-hydrogen-bonded NMA,³⁷ the $\pi \rightarrow \pi^*$ transition is much more extended over the molecule than previously thought.^{3b,37} In other words, the resonance Raman enhancements are not determined only by CN s.

Conclusions

We have measured the polarized and depolarized spectra of aqueous and neat NMA and NMAD in D₂O and decomposed these into single bands by a self-consistent spectral analysis. The depolarization ratios of all relevant bands were determined. The following results were obtained.

(1) The amide I and II bands of aqueous NMA can be decomposed into two subbands at 1626 and 1646, and 1565 and 1586 cm⁻¹, respectively. In accordance with an earlier study,¹¹ we assign the amide I pair to vibrational coupling between amide I vibrations and the HOH bending vibrations of water molecules hydrogen bonded to the NH and CO groups of the molecule, whereas the amide II pair is interpreted as arising from two NMA conformers differing in terms of the orientation of their *N*-methyl hydrogen atoms with respect to the NH group.

Amide I' of NMAD appears as a single band at 1626 cm⁻¹ due to absence of any vibrational coupling with the downshifted DOD bending modes. Amide II' consists of a doublet at 1493 and 1516 cm⁻¹, which results from a Fermi resonance interaction of amide II' with the combination of amide VI' (632 cm⁻¹) and a skeletal mode at 873 cm⁻¹.

(2) Amide I of neat NMA is composed of a highly polarized and an entirely depolarized subband at 1646 and 1658 cm⁻¹, respectively. This observation suggests that coupling between the transition dipole moments of the amide I vibrations in adjacent molecules of NMA oligomers causes a noncoincidence of the isotropic and anisotropic parts of their Raman scattering amplitudes.

(3) The rather broad unresolved band between 1420 and 1500 cm⁻¹ was decomposed into three nearly depolarized bands at 1434, 1453, and 1457 cm⁻¹, which by comparison with the results from the normal coordinate analysis (Table 1) could be assigned to the CCH₃ sb, NCH₃ oab, and NCH₃ ab modes, respectively. Another weak and polarized band at 1496 cm⁻¹ derives from the amide II mode of *cis*-NMA.^{3c,d,4}

(4) The depolarization ratios of amide III and CCH₃ sb of aqueous and neat NMA were found to be close to 0.33, independent of the excitation wavelength. Thus, these modes get their Raman intensity from the $\pi \rightarrow \pi^*$ transition even at visible excitation. Deuteration of the NH group eliminates the $\pi \rightarrow \pi^*$ contribution to CCH₃ sb and the band becomes depolarized. The polarized subbands of amide I, II, and II' as well as the single amide I' band exhibit a dispersion of their ρ values, indicating that in addition to the $\pi \rightarrow \pi^*$ other transitions at higher energies contribute significantly to their Raman cross sections. The intensity of the NCH₃ sb band is in part provided by the $\pi \rightarrow \pi^*$ transition and this enhancement increases by deuteration of the NH group. The antisymmetric methyl modes are nearly depolarized.

It is clear that a self-consistent decomposition of IR and IR and UV Raman spectra of NMA together with polarization measurements at different excitation wavelengths provide important new experimental results to improve our understanding of the normal modes and UV enhancement characteristics of this important molecule.

Acknowledgment. We gratefully acknowledge support from NIH Grant R01GM30741-12 to S.A.A. and NSF Grants MCB-9115906 and DMR-9110353 to S.K. Furthermore we thank Prof. Michael Morris for providing access to his computer facilities. R.S.-S. acknowledges fellowship support from the Max Kade foundation.

References and Notes

- (1) Katz, J. L.; Post, B. *Acta Crystallogr.* **1960**, *13*, 624.

- (2) (a) Radzicka, A.; Pedersen, L.; Wolfenden, R. *Biochemistry* **1988**, *27*, 4538. (b) Barker, R. H.; Boudreaux, G. J. *Spectrochim. Acta A* **1967**, *23A*, 727.
- (3) (a) Dudik, J. M.; Johnson, C. R.; Asher, S. A. *J. Phys. Chem.* **1985**, *89*, 3805. (b) Mayne, L. C.; Ziegler, L. D.; Hudson, B. *J. Phys. Chem.* **1985**, *89*, 3395. (c) Wang, Y.; Purrello, R.; Spiro, T. G. *J. Am. Chem. Soc.* **1989**, *111*, 8274. (d) Wang, Y.; Purrello, R.; Jordan, T.; Spiro, T. G. *J. Am. Chem. Soc.* **1991**, *113*, 6359, 6368.
- (4) Song, S.; Asher, S. A.; Krimm, S.; Shaw, K. D. *J. Am. Chem. Soc.* **1991**, *113*, 1155.
- (5) (a) Mirkin, N. G.; Krimm, S. *J. Am. Chem. Soc.* **1990**, *112*, 9016. (b) Mirkin, N. G.; Krimm, S. *J. Am. Chem. Soc.* **1991**, *113*, 9742.
- (6) Mirkin, N. G.; Krimm, S. *J. Mol. Struct.* **1991**, *242*, 143.
- (7) Miyazawa, T.; Shimanouchi, T.; Mizushima, S.-I. *J. Chem. Phys.* **1956**, *24*, 408.
- (8) Song, S.; Asher, S. A. *J. Am. Chem. Soc.* **1989**, *111*, 4295.
- (9) (a) Wang, Y.; Purrello, R.; Georgiu, S.; Spiro, T. G. *J. Am. Chem. Soc.* **1991**, *113*, 6368. (b) Mayne, L. C.; Hudson, B. *J. Phys. Chem.* **1991**, *95*, 2962.
- (10) Chen, X. G.; Asher, S. A.; Schweitzer-Stenner, R.; Mirkin, N. G.; Krimm, S., submitted for publication.
- (11) Chen, X. G.; Schweitzer-Stenner, R.; Mirkin, N. G.; Krimm, S.; Asher, S. A. *J. Am. Chem. Soc.* **1994**, *116*, 11141.
- (12) Fillaux, F.; DeLoze, C. *J. Chim. Phys.* **1976**, *73*, 1004.
- (13) Asher, S. A.; Bornett, B. W.; Chen, X. G.; Lemmon, D. H.; Cho, N.; Peterson, P.; Arrigoni, M.; Spirelli, L.; Cannon, J. *Appl. Spectrosc.* **1993**, *47*, 628.
- (14) Fukushi, K.; Kimura, M. *J. Raman Spectrosc.* **1979**, *8*, 125.
- (15) (a) Deb, S. K.; Bonsol, M. L.; Roy, A. P. *Appl. Spectrosc.* **1984**, *38*, 500. (b) Dreybrodt, W.; Stichternath, A. *Proceedings of the XIV-th International Conference on Raman Spectroscopy, Hong Kong*; Yu, N. T., Li, X.-Y., Eds.; Wiley & Sons: New York, 1994; p 1066.
- (16) Mirkin, N. G.; Krimm, S., to be submitted.
- (17) For the sake of simplicity we designate all methyl modes as symmetric and asymmetric C- or N-methyl bending vibrations (sb and ab), even though our normal coordinate analyses show that other local coordinates contribute to their PEDs and eigenvectors.
- (18) Harada, I.; Takeuchi, H. In: *Spectroscopy of Biological Systems*; Clark, R. T., Hester, R. E., Eds.; Wiley & Sons: New York, 1986; p 113.
- (19) Williams, R. W. *Biopolymers* **1992**, *32*, 829.
- (20) Herzberg, G. *Molecular Spectra and Molecular Structure. II. Infrared and Raman Spectra of Polyatomic Molecules*; Van Nostrand Reinhold: New York, 1945.
- (21) This equation can be easily derived from the mixed wavefunctions of the two vibrational states, which are obtained by diagonalizing the interaction matrix.²⁰
- (22) (a) Sokolowska, A.; Kecki, Z. *J. Raman Spectrosc.* **1993**, *24*, 331. (b) Kecki, Z.; Sokolowska, A. *J. Raman Spectrosc.* **1994**, *25*, 723.
- (23) Mirone, P.; Fini, G. *J. Chem. Phys.* **1979**, *71*, 2241.
- (24) Fini, G.; Mirone, P. *Spectrochim. Acta A* **1976**, *32*, 625.
- (25) Jones, D. R.; Wang, C. H.; Christensen, D. H.; Nielsen, O. F. *J. Chem. Phys.* **1976**, *64*, 4475.
- (26) Perchard, C.; Perchard, J. P. *J. Raman Spectrosc.* **1975**, *6*, 74.
- (27) Mortensen, A.; Faurskov-Nielsen, O.; Yarwood, J.; Shelley, V. J. *Phys. Chem.* **1994**, *98*, 5221.
- (28) Thomas, H. D.; Jonas, J. *J. Chem. Phys.* **1989**, *90*, 4144.
- (29) (a) Döge, G. Z. *Naturforsch.* **1973**, *28a*, 919. (b) Wang, C. H.; McHale, J. *J. Chem. Phys.* **1980**, *72*, 4039. (c) McHale, J. L. *J. Chem. Phys.* **1981**, *75*, 30. (d) Logan, D. C. *J. Chem. Phys.* **1986**, *103*, 215. (e) Logan, D. C. *J. Chem. Phys.* **1989**, *131*, 199.
- (30) Torii, H.; Tasumi, M. *J. Chem. Phys.* **1993**, *99*, 8459.
- (31) Kirillov, S. *J. Raman Spectrosc.* **1993**, *24*, 167.
- (32) Vanderginste, B. G. M.; DeGalan, L. *Anal. Chem.* **1975**, *47*, 2124.
- (33) (a) Bradley, M.; Zerda, T. W.; Jonas, J. *Spectrochim. Acta A* **1984**, *40A*, 1117. (b) Sokolowska, A. *J. Raman Spectrosc.* **1987**, *18*, 513.
- (34) (a) Long, D. A. *Raman Spectroscopy*; McGraw-Hill: New York, 1977. (b) Udagawa, Y.; Iijima, M.; Ito, M. *J. Raman Spectrosc.* **1974**, *2*, 315.
- (35) (a) Garozzo, M.; Galluzzi, F. *J. Chem. Phys.* **1975**, *64*, 1720. (b) Peticolas, W. L.; Blazej, D. C. *J. Chem. Phys. Lett.* **1979**, *63*, 604. (c) Warshel, A.; Dauber, P. *J. Chem. Phys.* **1977**, *66*, 5477.
- (36) Jordan, T.; Spiro, T. G. *J. Raman Spectrosc.* **1994**, *25*, 537.
- (37) Hudson, B. S. *Proc. LALS Conf.*, in press.